Lab on a Chip

Cite this: *Lab Chip*, 2012, **12**, 1865

www.rsc.org/loc

PAPER

Elastomeric microposts integrated into microfluidics for flow-mediated endothelial mechanotransduction analysis†

Raymond H. W. Lam,[abc] Yubing Sun,[ab] Weiqiang Chen[ab] and Jianping Fu*[abd]

Received 22nd November 2011, Accepted 24th February 2012
DOI: 10.1039/c2lc21146g

Mechanotransduction is known as the cellular mechanism converting insoluble biophysical signals in the local cellular microenvironment (*e.g.* matrix rigidity, external mechanical forces, and fluid shear) into intracellular signalling to regulate cellular behaviours. While microfluidic technologies support a precise and independent control of soluble factors in the cellular microenvironment (*e.g.* growth factors, nutrients, and dissolved gases), the regulation of insoluble biophysical signals in microfluidics, especially matrix rigidity and adhesive pattern, has not yet been achieved. Here we reported an integrated soft lithography-compatible microfluidic methodology that could enable independent controls and modulations of fluid shear, substrate rigidity, and adhesive pattern in a microfluidic environment, by integrating micromolded elastomeric micropost arrays and microcontact printing with microfluidics. The geometry of the elastomeric micropost array could be regulated to mediate substrate rigidity and adhesive pattern, and further the elastomeric microposts could be utilized as force sensors to map live-cell subcellular contractile forces. To illustrate the general application of our methodology, we investigated the flow-mediated endothelial mechanotransduction process and examined specifically the involvement of subcellular contractile forces in the morphological realignment process of endothelial cells under a sustained directional fluid shear. Our results showed that the cytoskeletal contractile forces of endothelial cells were spatiotemporally regulated and coordinated to facilitate their morphology elongation process along the direction of flow. Together, our study provided an integrated microfluidic strategy to modulate the *in vitro* cellular microenvironment with both defined soluble and insoluble signals, and we demonstrated its application to investigate quantitatively the involvement of cytoskeletal contractile forces in the flow-mediated mechanotransduction process of endothelial cells.

Introduction

In the local cellular microenvironment, insoluble biophysical cues other than soluble factors, such as extracellular mechanical forces and mechanical properties of the extracellular matrix (ECM), can contain important regulatory signals to direct cellular behaviors.[1–4] For example, extracellular mechanical forces including fluid shear stress and cell stretch forces can mediate the endogenous actomyosin-based intracellular cytoskeleton (CSK) contractile forces.[5] This CSK force (sometimes referred to as CSK tension or contractility[5]) is transmitted through the CSK structure to the cell–ECM adhesion sites, or focal adhesions (FAs) that are physically associated with the CSK structure to form the CSK–FA–ECM mechanical linkage. The altered intracellular CSK contractility leads to changes of the molecular composition, structure, and dynamics of FAs, and it can further mediate the force-sensitive adhesion signaling to form a feedback mechanism to regulate in turn the CSK contractility, to achieve a force balance between the endogenous CSK contractility and external mechanical forces transmitted across the cell–ECM adhesions.[2–5] Indeed, such tensional homeostasis in the intracellular CSK structure plays a key role in the regulation of basic cellular functions,[6,7] such as cell proliferation,[8,9] apoptosis,[10] adhesion,[11] and migration.[12,13] Dysregulation of tensional homeostasis in cells contributes to pathogenesis of several human diseases, such as atherosclerosis,[14–16] osteoarthritis and osteoporosis,[17,18] and cancer.[19] The process to convert extracellular insoluble biophysical signals into intracellular biochemical events and ultimately the functional and behavioral responses of cells is often referred to as 'mechanotransduction'.

In human vascular system, the endothelium is the thin layer of endothelial cells (ECs) that lines the interior surface of blood vessels, forming an interface between circulating blood in the

[a]*Integrated Biosystems and Biomechanics Laboratory, University of Michigan, Ann Arbor, MI 48109, USA. E-mail: jpfu@umich.edu; Fax: +1-734-647-7303; Tel: +1-734-615-7363*
[b]*Department of Mechanical Engineering, University of Michigan, Ann Arbor, MI 48109, USA*
[c]*Department of Mechanical and Biomedical Engineering, City University of Hong Kong, Hong Kong, People's Republic of China*
[d]*Department of Biomedical Engineering, University of Michigan, Ann Arbor, MI 48109, USA*
† Electronic supplementary information (ESI) available. See DOI: 10.1039/c2lc21146g

lumen and the rest of the vessel wall. The ECs are continuously exposed to the hemodynamic factors including fluid shear stress and circumferential cell stretching that drive the viscous blood flow and control lumen diameter. The principal functions of endothelium are the maintenance of anticoagulant properties, the physiological control of lumen diameter, the regulation of vascular permeability, and the pathological consequences associated with acute inflammation, wound healing, and cardiovascular disorders such as the focal localization of atherosclerosis.[20] In all of these processes, hemodynamic factors can influence endothelial biology either by the direct action of shear stress and stretch forces on the endothelium itself or by indirect modification of the local concentrations of chemicals and agonists at the endothelial luminal surface, thereby influencing the association between these molecules and their endothelial receptors.[20,21]

Mechanically related responses controlled by the endothelium have evolved as part of the normal vascular physiology. It has been suggested that a potential mechanism for direct shear stress-induced mechanotransduction in ECs may occur sequentially by[20,21] (1) local displacement of mechanosensors at the EC luminal surface, (2) force transmission *via* the CSK structure to distribute the mechanical stress throughout the cell, followed by (3) transduction of the transmitted stress at the mechanotransductive CSK-linked FA sites remote from the shear-sensing sites. Thus ECs are always under CSK tension and respond to changes of CSK tension through force-sensitive FA signaling, which can lead to adaptive cellular responses such as CSK reorganization, changes of cellular mechanics, and morphological and functional responses of ECs.[22–25]

As mechanotransduction is crucial to EC functions, its dysregulation can lead to pathological conditions in ECs where an abnormal tensional state develops to affect the intricate CSK–FA–ECM linkage and thus FA signaling. For example, sustained irregularities in blood flow at the branch structures of the arterial network are pathological to the endothelium and can cause abnormal remodeling of the EC structure and dysregulation of the EC CSK contractility, which in turn leads to chronic inflammation and subsequently develops into atherosclerotic plaques and other cardiovascular diseases.[26–28] In addition, inadequate chronic shear can cause apoptosis of ECs, abnormal vascular permeability and endothelium regression, all of which are in part related to dysregulation of the adaptive CSK structure and contractility in ECs.[29,30] Together, it appears that adaptive modulations of CSK structure and contractility are critically involved in the flow mediated endothelial mechanotransduction process. Thus, a better understanding of dynamics of the CSK contractility during the flow-mediated endothelial mechanotransductive process will help elucidate the mechanotransductive system in ECs and thus contribute to our understanding of flow-induced vascular disease processes.

Over the last decade, various microfluidic platforms have been established as *in vitro* models to precisely control the vascular culture microenvironment in order to quantitatively investigate different flow-mediated endothelial processes.[18,31–38] These microfluidic platforms typically contain straight microfluidic channels or wells whose critical dimensions are comparable to lumen diameters of human blood vessels (ranging from microns to millimetres). Majority of these microfluidic EC culture systems incorporate fluid flow over adhered, confluent EC monolayers to mimic the hemodynamic shear stress experienced by ECs in their native environment. These reported microfluidic EC culture platforms have been applied successfully to study alignment and elongation of ECs under fluid shear,[31] nitric oxide production by ECs stimulated with adenosine triphosphate,[18,32] adhesion properties of ECs under fluid shear,[33,37] adhesion of platelets to ECs,[34] endothelial permeability,[35,38] and intravascular adhesion of metastatic breast cancer cells to ECs.[36] To date, however, microfluidic systems that can apply well-controlled shear stress while simultaneously reporting the adaptive dynamic CSK contractile response of ECs have not yet been realized, and the current research was set to specifically address this significant technical gap.

To aid in the investigation of the flow-mediated endothelial mechanotransduction process, herein we reported for the first time a soft lithography-compatible microfluidic strategy to apply a uniform laminar shear stress to live single ECs and simultaneously monitor their adaptive CSK contractile response by using a microfabricated array of silicone elastomeric microposts integrated onto the bottom surface of a microfluidic channel. More specifically, our microengineered EC culture device, or the 'micropost array in a channel' (μPAC) device, consisted of a microfluidic cell culture channel and an array of hexagonally spaced poly(dimethylsiloxane) (PDMS) microposts embedded at the bottom surface of the microfluidic channel (Fig. 1 and 2a and b). Importantly, the PDMS microposts can serve as sensitive force sensors to report live-cell subcellular CSK contractility of ECs at the single-FA level during the flow-mediated endothelial mechanotransduction process.[39–41] In addition, by modulating the geometry of the PDMS micropost array, the mechanical property of the PDMS micropost array can be regulated to control the effective modulus of the microfluidic channel to which ECs are adhered.[41,42] (Readers are referred to ref. 43 for more details on the PDMS micropost array.)

The PDMS micropost array can be functionalized with adhesive ECM proteins using microcontact printing to control the adhesive ECM pattern and ECM ligand density.[42,43] However, the oxygen plasma-assisted PDMS–PDMS bonding process, necessary for sealing the microfluidic channel of the μPAC device, can cause a significant challenge owing to removal of proteins on the PDMS surface during plasma conditioning of the PDMS surface. To address this issue, in this work we developed a modified microcontact printing method to protect protein molecules coated on the PDMS micropost tops from the attack of the oxygen plasma during the channel-sealing step for the μPAC device. Thus, the μPAC device could allow independent controls of both soluble factors (*e.g.* by using pre-conditioned cell media) and insoluble biophysical signals, including shear stress, substrate rigidity, adhesive ECM pattern, and ECM ligand density, for ECs seeded in the microfluidic channel.

Methods

Device fabrication

The μPAC device was fabricated using soft lithography and replica molding of PDMS. Three silicon mold masters (each for the micropost array, microfluidic channel, and stamp for microcontact printing) were microfabricated prior to PDMS casting. The silicon

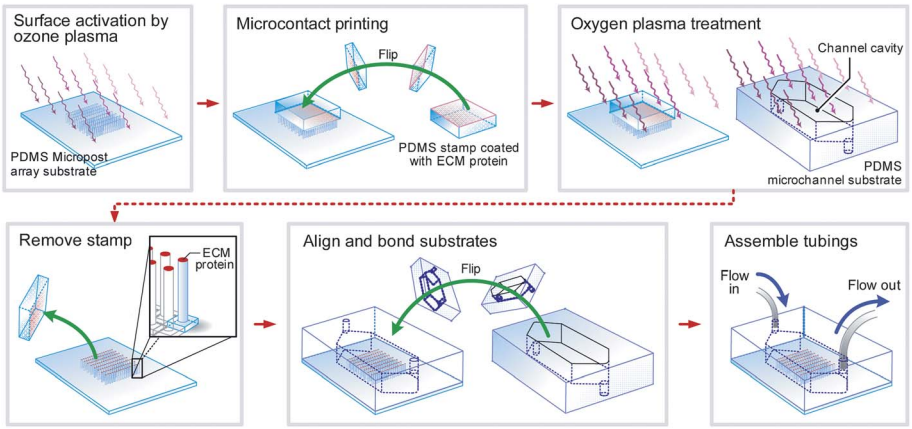

Fig. 1 Schematic of the fabrication process for the μPAC device. The μPAC device was fabricated using a soft-lithography compatible fabrication technique, and it contained a rectangular microfluidic channel embedded with a hexagonally arranged PDMS micropost array on the bottom surface of the microfluidic channel. Using microcontact printing, the tops of the PDMS microposts were selectively coated with adhesive ECM proteins for cell seeding.

wafers were first primed with the adhesion promoter, hexamethyldisilazane (HMDS, AZ Electronic Materials, Branchburg, NJ), and spin-coated with a photoresist (AZ5214, AZ Electronic Materials). The photoresist layer was then patterned using contact or projection photolithography. The exposed regions of the silicon wafers were etched using deep reactive ion etching (DRIE; STS Deep Silicon Etcher, Surface Technology Systems, Newport, UK) with a target depth between about 10 and 100 μm (for the micropost array: 9 μm; for the microfluidic channel: 100 μm; for the microcontact printing stamp: 40 μm). After stripping the photoresist, the surfaces of the silicon masters were activated by an oxygen plasma treatment (medium: air, pressure: 700 mTorr, energy: 1 kJ; Plasma Prep II, SPI Supplies, West Chester, PA) before being silanized with (tridecafluoro-1,1,2,2,-tetrahydrooctyl)-1-trichlorosilane vapor (United Chemical Technology, Bristol, PA) for 2 h, in order to facilitate subsequent release of PDMS from the silicon masters after the molding process.

Replica molding of PDMS was utilized to cast three different substrates: (1) the micropost array, (2) the microfluidic channel, and (3) the microcontact printing stamp. PDMS prepolymer (Sylgard-184, Dow Corning, Midland, MI) was prepared first by thoroughly mixing the monomer with the curing agent (with the w/w ratio of 10 : 1). During the casting process, the PDMS prepolymer was poured onto the silicon molds and baked at 110 °C for 20 h. Fully cured PDMS substrates were peeled off from the silicon molds, and the excessive PDMS was trimmed using a razor blade. It is worth noting that the microfluidic channel and microcontact printing stamp substrates were both prepared by single casting, while the PDMS micropost array was fabricated using a 'double casting' process to ensure a planar surface of the PDMS micropost tops.[43] In brief, the first PDMS substrate cast from the silicon micropost array master would serve as a negative mold and was subsequently plasma-treated, silanized, and applied to cast the secondary PDMS micropost array on a glass coverslip (VWR, Radnor, PA). After peeling off from the negative PDMS mold, collapsed PDMS microposts were rescued by sonication in 100% ethanol for 30 s followed by dry-release with liquid CO_2 using a critical point dryer (Samdri®-PVT-3D, Tousimis, Rockville, MD).

Fig. 1 shows a diagram of the fabrication process for the μPAC device. (A more detailed fabrication process is shown in Fig. S1†.) The PDMS stamp was first inked with a fibronectin solution (BD Biosciences, San Jose, CA) for 1 h at a concentration of 50 μg mL^{-1} in distilled water, followed by aspiration and blown dry with nitrogen gas. Surface activation of the PDMS micropost array was achieved using ultraviolet ozone (UV-ozone cleaner, Jelight, Irvine, CA) for 7 min, in order to ionize the PDMS surface and thus facilitate transfer of ECM molecules from the stamp to the PDMS micropost tops. Oxygen plasma and UV ozone are commonly used for surface activation of PDMS, and their main difference is that UV ozone treatment is a milder process and thus can be better controlled.[44] The fibronectin-coated stamp was then gently placed on the PDMS micropost array for 30 s to transfer ECM proteins onto the PDMS micropost tops. Prior to removal of the PDMS stamp, both the PDMS micropost array and the microchannel substrate (with an inlet and an outlet generated by punching holes at the channel terminals; Harris Uni-Core Dia. 0.5 mm, Ted Pella, Redding, CA) were treated with the oxygen plasma (medium: air, pressure: 700 mTorr; energy: 1 kJ) for surface activation. To assemble the μPAC device, the microcontact printing stamp was removed from the PDMS micropost array, and the microfluidic channel substrate was then aligned and bonded onto the PDMS micropost array by hand under a dissection stereomicroscope. Prior to experiments, the μPAC device was stored in a refrigerator at 4 °C for at least 2 days to eliminate the effect of surface activation. Proteins coated in the μPAC device can retain their activities for at least 1 week when the μPAC device is stored at 4 °C.[43] Silicone tubing (Tygon tubing EW-06418-02, Cole-Parmer, Vernon Hills, IL) and adaptors (Cat# NE-1310-02, New England Small Tube, Litchfield, NH) were then inserted into the inlet and outlet of the microfluidic channel for fluidic connections.

Quantification and simulation of fluid flow

The cell culture media can be safely treated as a Newtonian fluid. Thus, shear stress τ_o exerted on cells adhered on the PDMS

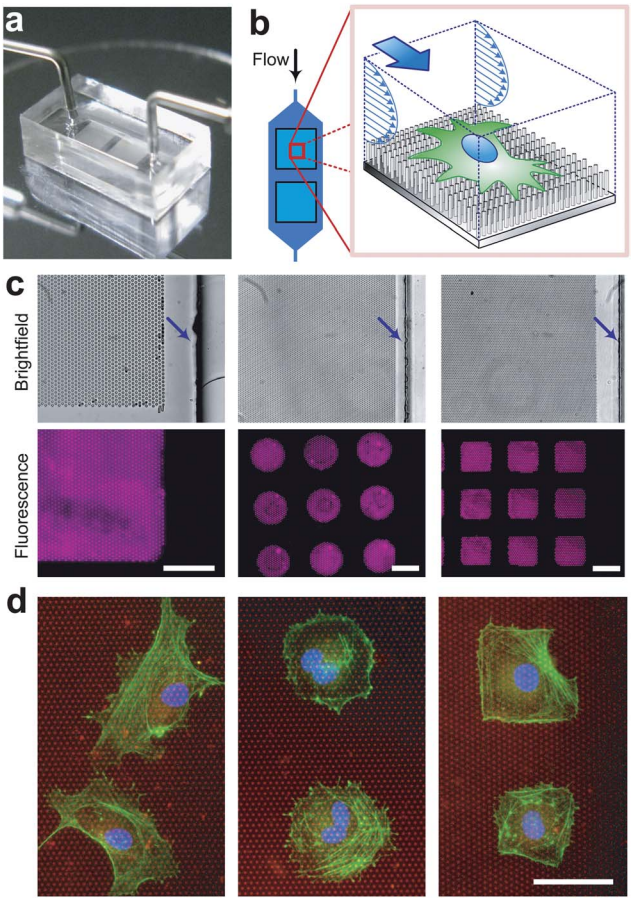

Fig. 2 The μPAC device with the microfluidic channel embedded with the PDMS micropost array coated with different patterns of adhesive ECM molecules. (a) The μPAC device (dimensions: 10 mm (*l*) × 5 mm (*w*) × 4 mm (*h*)) connected with external tubing for the fluid supply and control. (b) Cartoon of a single cell plated on the PDMS microposts and the cell culture medium flowing continuously along the microfluidic channel to exert fluid shear stress on the cell. (c) Brightfield microscopic images (*top row*) and corresponding fluorescence images (*bottom row*) of the PDMS micropost array coated with different patterns of fluorescence-labeled BSA (*left*: uniform coating, *middle*: an array of circles, and *right*: an array of squares). Arrows indicate locations of the microfluidic channel walls. Scale bar, 50 μm. (d) Immunostaining images of single HUVECs plated on the PDMS micropost arrays coated with different adhesive patterns of fibronectin (*left*: uniform coating, *middle*: an array of circles, and *right*: an array of squares). The PDMS microposts were labeled with DiI (*red*), while HUVECs were stained for the nucleus (*blue*) and actin microfilaments (*green*). Scale bar, 50 μm.

microposts can be calculated approximately using the expression of $\tau_o = (4\mu V_{max})/H = (6\mu Q)/(WH^2)$, where μ is the viscosity of the culture media ($\sim 10^{-3}$ Pa s), V_{max} is the maximum flow velocity within the microfluidic channel, Q is the volume flow rate of the culture medium, and W and H are the microfluidic channel width and height, respectively.

We further applied the simulation software COMSOL 4.1 (COMSOL, Burlington, MA) using an iterative computation approach to quantify the flow and shear stress profiles within the microfluidic channel. A microfluidic channel unit, which was repeatedly distributed over the microfluidic channel in the μPAC device, was considered in the simulation (see ESI†).

Cell culture

Human umbilical vein endothelial cells (HUVECs, Cat# CC-2583, Lonza, Walkersville, MD) were cultured using the endothelial basal medium (EBM-2, Cat# CC-3156, Lonza) with additional soluble factors (EGM-2, Cat# CC-4176, Lonza) including hEGF, VEGF, hFGF-B, R3-IGF-1, heparin, ascorbic acid, hydrocortisone, gentamicin, amphotericin-B, and fetal bovine serum (FBS). After cells became confluent, they were trypsinized (0.05% w/v trypsin in EDTA) and subcultured with a plating density of 5×10^3 cells per cm^2. Only early passages of HUVECs (passage 4–7) were used in our assays.

Device pre-conditioning and cell seeding

The microfluidic channel in the μPAC device was sequentially flushed with 100% and 50% ethanol and then distilled water to gradually hydrate the channel. To label the PDMS microposts, 10 μg mL^{-1} 1,1′-dioctadecyl-3,3,3′3′-tetramethylindocarbocyanine perchlorate (DiI, Invitrogen, Carlsbad, CA) in distilled water was flushed through the microfluidic channel for 1 h. After purging the microfluidic channel with distilled water for another 1 h, Pluronics F127 NF (0.2% w/v in distilled water; P2443-250G, Sigma-Aldrich, St. Louis, MO) was flushed through the microfluidic channel for 30 min. Distilled water and phosphate buffered saline (PBS) were applied sequentially to remove free DiI molecules in the microfluidic channel, followed by replacing PBS with the fresh cell culture medium. The μPAC device was then incubated for about 1 h at 37 °C and 5% CO_2 before seeding cells.

HUVECs were seeded into the microfluidic channel at a density of 2×10^4 cells per cm^2 under a slow stream of the fresh culture medium driven by a syringe pump (0.005 mL min^{-1}; NE-300, Pump Systems, Farmingdale, NY). After plating cells in the μPAC device, they were cultivated in an incubator at 37 °C and 5% CO_2 for more than 2 h for complete cell attachment. Using $\tau_o = (4\mu V_{max})/H = (6\mu Q)/(WH^2)$, the shear stress τ_o exerted on cells during cell seeding was estimated to be about 0.25 dyne cm^{-2}, small enough not to affect attachments of cells to the PDMS microposts.

Observation of shear-mediated EC responses

After cell seeding, the μPAC as well as the control microfluidic device without the PDMS microposts were continuously supplied with fresh cell culture media for 6 h to generate a steady directional shear stress of 20 dyne cm^{-2}, a level experienced typically for human vascular endothelium *in vivo*.[21,45–47] Live single ECs were continuously monitored for 6 h under fluorescence microscopy (Zeiss Observer Z1, Carl Zeiss Microscopy, Hertfordshire, UK) enclosed in an environmental incubator (XL S1, Carl Zeiss Microscopy) to maintain the experimental environment at 37 °C and 5% CO_2.

Quantification of EC morphological and contractile responses to shear stress

Live single ECs were randomly chosen in the μPAC device for our quantitative studies. Time-lapse fluorescent images of the PDMS micropost tops underneath single live ECs were taken every 1 h during the live-cell experiments. We further recorded

the brightfield images of the ECs during their morphological realignment response to shear stress. The fluorescent images were analyzed for cellular contractility using a customized MATLAB program (Mathworks, Novi, MI).[43] Briefly, to quantify deflections x_p of the tops of the bended PDMS microposts, their original undeflected positions were determined first using an automated shape fitting algorithm with interpolations from unattached free-standing PDMS microposts surrounding the cell region.[43] Each x_p was then converted to a local horizontal traction force f_p using the expression of $f_p = Kx_p$, where K was the nominal spring constant of the PDMS micropost calculated from the *Euler–Bernoulli* beam equation (see discussion in the Results and discussion). Total cellular contractility was quantified as the sum of the absolute magnitudes of local traction forces exerted on all the PDMS microposts underneath the whole single ECs.

The temporal dynamics of the shear-induced morphological realignment process of HUVECs was quantified using the time-lapse brightfield microscopic images and a shape directionality S defined as $S = (S_x - S_y)/(S_x + S_y)$, where $S_x = \sum_{i,j\forall(i,j)\in \text{cell}} |i - C_x|$ and $S_y = \sum_{i,j\forall(i,j)\in \text{cell}} |j - C_y|$, and (C_x, C_y) is the geometric center of the cell in the pixel unit defined as $C_x = \sum_{i,j\forall(i,j)\in \text{cell}} i/N_{\text{pixel}}$ and $C_y = \sum_{i,j\forall(i,j)\in \text{cell}} j/N_{\text{pixel}}$. Here the x- and y-axis indicated the two orthogonal directions parallel and perpendicular to the flow direction, respectively, i and j were the pixel indices in the x- and y-directions, respectively, and N_{pixel} was the total number of pixels covered by the whole cell spread area. Note that only the pixels within the cell spread area were considered in this calculation. Thus, the shape directionality S approaches a value of 1 if the cell body is perfectly aligned with the flow direction, and $S = -1$ if the cell body is along the y-axis and thus completely perpendicular to the flow direction. Cells with no directional preference in their morphology (such as cells with a spherical shape) have a shape directionality $S = 0$.

To characterize the spatiotemporal distribution and regulation of subcellular CSK contractility during the shear-mediated endothelial realignment process, we defined a force directionality D as a function of the absolute total contractile forces parallel (D_x) and perpendicular (D_y) to the flow direction, and $D = (D_x - D_y)/(D_x + D_y)$, where $D_x = \sum_{p,q\forall(p,q)\in \text{cell}} |f_x(p,q)|$ and $D_y = \sum_{p,q\forall(p,q)\in \text{cell}} |f_y(p,q)|$, and p and q were the PDMS micropost indices in the x- and y-directions, respectively, and $f_x(p, q)$ and $f_y(p, q)$ were contractile force components measured for individual PDMS microposts in the x- and y-directions, respectively. Thus, the force directionality D indicates whether subcellular contractile forces would be distributed primarily along the direction of the flow ($0 < D \leq 1$) or perpendicular to the flow direction ($-1 \leq D < 0$).

Immunofluorescence staining

HUVECs were fixed in the μPAC device by first flowing 4% (w/v) paraformaldehyde (PFA, Electron Microscopy Science, Hatfield, PA) in PBS through the cell-seeded microfluidic channel for 30 min. The PDMS microfluidic channel substrate was then peeled off from the PDMS micropost array. The PDMS micropost array was then rinsed thoroughly with PBS and soaked in a blocking solution (10% goat serum in PBS; Invitrogen) for 1 h to eliminate non-specific binding in the following staining step. After rinsing with PBS, cells on the PDMS microposts were stained with 4′,6-diamidino-2-phenylindole (DAPI, 20 nM, Invitrogen) and Alexa Fluor-647 labelled phalloidin (0.4 μM, Invitrogen) in the blocking solution for 1 h for visualization of the nucleus and filamentous actin, respectively.

Results and discussion

Microfluidic design and patterning of adhesive molecules

In this work, we developed an integrated μPAC device using a soft lithography-compatible fabrication technique, which contained a rectangular microfluidic channel embedded with an array of hexagonally arranged PDMS microposts (Fig. 1 and 2a and b). The microposts could serve simultaneously as sensitive force sensors to map live-cell subcellular traction forces, a critical component involved in the cellular mechano-sensing and -transduction process.[5]

Conventional methods to control substrate rigidity for regulating mechanoresponsive cellular behaviors have largely relied on natural or synthetic hydrogels. However, these natural or synthetic hydrogels cannot be incorporated readily into conventional PDMS-based microfluidic devices. Recently, our group and others have proposed the idea to use geometrically modulated PDMS micropost arrays to regulate substrate rigidity independently of effects on adhesive and other material surface properties.[39–41] The spring constant K of the PDMS micropost is solely determined by its geometry and by the *Young*'s modulus E of PDMS, and K can be approximately calculated using the *Euler–Bernoulli* beam theory as $K = 3\pi ED_p^4/(64L_p^3)$, where D_p and L_p are the PDMS post diameter and height, respectively.[39–41] The substrate rigidity of the PDMS micropost array can be further characterized using an effective *Young*'s modulus E_{eff} of a continuous elastic substrate, and E_{eff} is calculated as $E_{\text{eff}} = 9K/(2\pi D_p)$.[40] Thus, the rigidity of the PDMS micropost array can be modulated simply by varying the post height L_p and diameter D_p while keeping all other aspects of the substrate such as surface chemistry, ligand density, and bulk and nanoscale mechanics of the PDMS unchanged. In our previous studies, we have shown that the rigidity of the PDMS micropost array can significantly impact cell morphology, FA formation, CSK contractility, and stem cell differentiation.[41,42] Thus, by modulating the geometry of the PDMS micropost array in the μPAC device, the substrate rigidity of the microfluidic channel on which ECs were adhered could be regulated. In our current μPAC device, the diameter D_p and height L_p of the PDMS micropost were about 1.83 μm and 9 μm, respectively, and the center-to-center spacing between the microposts was 4 μm. The spring constant K and the corresponding effective modulus E_{eff} of the PDMS micropost array were 2.3 nN μm^{-1} and 1.62 kPa, respectively.

Our integrated fabrication technique for the μPAC device further allowed patterning of adhesive ECM molecules inside a microfluidic environment, which has been a significant technical challenge preventing a well-controlled cellular adhesive environment inside microfluidic devices.[48] Surface activation of

PDMS using the oxygen plasma is normally required for PDMS–PDMS bonding to seal PDMS-based microfluidic channels. However, this plasma treatment can remove a significant amount of adhesive proteins coated on the PDMS surface, preventing using the strategy of coating the PDMS surface with adhesive proteins prior to the plasma-assisted PDMS–PDMS bonding process. To confirm the deteriorative effect of the oxygen plasma treatment on protein coating, we performed control assays using Alexa 555 conjugated-bovine serum albumin (Cy3-BSA; Cat# A13100, Invitrogen) printed on the PDMS micropost tops. Indeed, our assays showed that even a short treatment of the oxygen plasma in tens of seconds could remove a significant amount of BSA coated on the PDMS micropost tops (Fig. S2†). To circumvent this problem, in our μPAC fabrication process, the PDMS microcontact printing stamp was used to protect ECM proteins in the contact regions from attacks of the oxygen plasma during the PDMS surface activation process (Fig. 1). Fig. 2c and d demonstrate the effectiveness of our fabrication method to coat different patterns of fibronectin (an adhesive ECM protein) in the microfluidic channel of the μPAC device. The morphologies of single HUVECs plated onto the PDMS micropost array could be controlled using such patterned adhesive islands. When a low density of HUVECs were injected into the μPAC device, the cells would attach only to the ECM coated PDMS microposts and spread to conform to different geometries of the adhesive islands.

The μPAC device could be used for simultaneous regulations of soluble (including growth factors, nutrients, and dissolved gases) and insoluble signals (such as shear stress and substrate rigidity) in the cellular microenvironment. For example, the soluble biochemical factors could be supplied using a continuous flow of preconditioned culture media injected into the μPAC device. The dissolved gases in the culture media could be regulated either by preconditioning or by controlling the gaseous environment surrounding the μPAC device. Thus, the gases could penetrate through the gas-permissible PDMS to regulate concentrations of the dissolved gases in the culture media.[48,49] Flow rate of the cell culture media in the microfluidic channel could be controlled to regulate fluid shear stress exerted on cells adhered on the PDMS microposts. Our fabrication method for the μPAC device further allowed the microfluidic channel to be functionalized with adhesive ECM patterns, thus enabling studies of cell shape and adhesion-mediated cellular behaviors in a microfluidic environment.[50–53] Together, the μPAC device could provide an effective means for spatiotemporal control of both soluble and insoluble cues in the cellular microenvironment to direct cellular responses, by combining surfaces that mimic complex biochemistries and geometries and mechanics of the ECM with microfluidic channels that regulate transport of soluble factors and shear stress exerted on the cells.

Flow characteristics

HUVECs could spread and flatten out on the PDMS micropost array after the initial cell seeding and incubation steps. Thus, the shear stress exerted on HUVECs plated in the μPAC device could be estimated using the expression $\tau_o = (4\mu V_{max})/H = (6\mu Q)/(WH^2)$. By modulating the volume flow rate Q and thus the maximum flow velocity V_{max}, we could control the magnitude of the shear stress τ_o exerted on HUVECs seeded in the μPAC device.

To determine whether shear stress would cause deflection of free PDMS microposts that were not adhered by HUVECs, we first performed computational analysis using the simulation software COMSOL 4.1 to calculate flow velocity and shear stress in the μPAC device. We selected a rectangular parallelepiped-shaped repeating element as the simulation unit (with the unit length of 6.93 μm, width of 4 μm, and height of 109 μm), which was composed of two halves of the PDMS microposts (Fig. 3a). Boundary conditions of this simulation unit were set as periodic for its entrance and exit faces and symmetry along its two side faces. A no-slip boundary condition was assigned to all other PDMS surfaces, *i.e.* the ceiling and bottom surface of the microfluidic channel and the tops and shafts of the PDMS microposts. Our simulation results demonstrated a relatively large change of flow velocity right above the micropost tops (Fig. 3b), suggesting that shear stress exerted on the PDMS micropost was concentrated at the micropost top. This observation was confirmed in Fig. 3c where the calculated shear stress at different horizontal planes along the height of the PDMS micropost was shown. From these simulation results, we determined that the maximum shear stress on the PDMS micropost top was about $\tau_o \approx 40 \times V_{max.}$. Hence, the shear stress required to initiate re-alignment of ECs, which is typically between 1 and

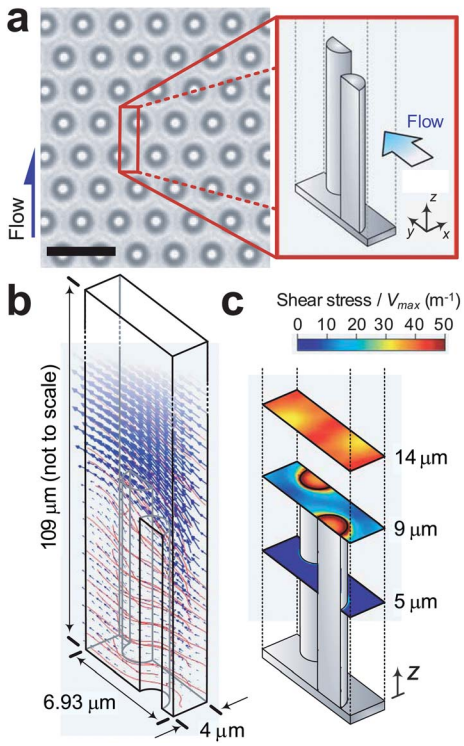

Fig. 3 Simulation of flow characteristics in the microfluidic channel of the μPAC device. (a) Brightfield microscopic image of the PDMS micropost array embedded at the bottom of the microfluidic channel of the μPAC device. The inset shows the repeating geometrical unit used for flow simulation. Scale bar, 6 μm. (b) Simulation results of flow velocity (*blue arrows*) and streamlines (*red curves*) around the PDMS microposts. (c) Colorimetric maps showing magnitudes of the shear stress at different horizontal planes along the height of the PDMS microposts as indicated.

100 dyne cm^{-2},[54] would cause a negligible deflection (<15 nm) of the PDMS micropost used in this work. We had further performed control assays to confirm that the maximum volume flow rate applied in our experiments would not induce any measurable deflection of free PDMS microposts that were not attached by cells (Fig. S3†).

Morphological response of HUVECs to shear stress

Morphological realignment of ECs has been observed in different studies as one of the mechanoresponsive behaviors of ECs in response to sustained directional fluid flow. Using the μPAC device as well as a control microfluidic device with a flat microfluidic channel, we performed cell shearing experiments to elicit and quantify the morphological realignment response of HUVECs.

Before cell shearing assays, the morphology of HUVECs remained random in orientation and relatively round in shape (Fig. 2d, left), whereas the morphology of HUVECs after a 6 h shearing stimulation with $\tau_o = 20$ dyne cm^{-2} became aligned and elongated in the direction of flow as shown by both the immunofluorescence staining and scanning electron microscopy (SEM; Hitachi SU8000, Hitachi High Technologies America, Inc., Pleasanton, CA) images (Fig. 4a and b and Fig. S4†). Fig. 4c plots the temporal evolutions of the shape directionality and normalized cell area of individual HUVECs during the 6 h shearing stimulation with $\tau_o = 20$ dyne cm^{-2}. From Fig. 4c, it appears that HUVECs plated on both the PDMS microposts and the flat PDMS surface progressively aligned and elongated in the direction of flow with time after the onset of cell shearing assays. The curve of the shape directionality S initially increased quickly with time and then leveled off. More specifically, the shape directionality S increased rapidly from 0 to about 0.23 within the first 4 h of the cell shearing experiments. After this initial 4 h period of rapid morphological realignment of HUVECs, the shape directionality S reached a plateau with the maximum of about 0.23, comparable to previously reported data.[55,56] Interestingly, we further observed that during the morphological realignment of HUVECs, their overall cell spread area remained largely unchanged (within ±10% of the initial cell area; Fig. 4c, right). Thus, it appeared that during their morphological realignment process, HUVECs could actively extend their cell body length along the direction of the flow while simultaneously contract in the direction perpendicular to the flow (Fig. S5†).

Response of cellular contractility of HUVECs to shear stress

The shear-mediated endothelial realignment process shown in Fig. 4c strongly implicated involvements of CSK remodeling and adaptive CSK contractile response in regulating the mechanoresponsive behaviors of ECs in response to a sustained directional shear stress, as the CSK structure and contractility are the major intracellular components regulating dynamic changes of cell morphology. To characterize CSK contractile dynamics of HUVECs during their morphological realignment, we utilized the PDMS microposts as live-cell force sensors to simultaneously measure spatiotemporal CSK contractile dynamics (Fig. 5a).

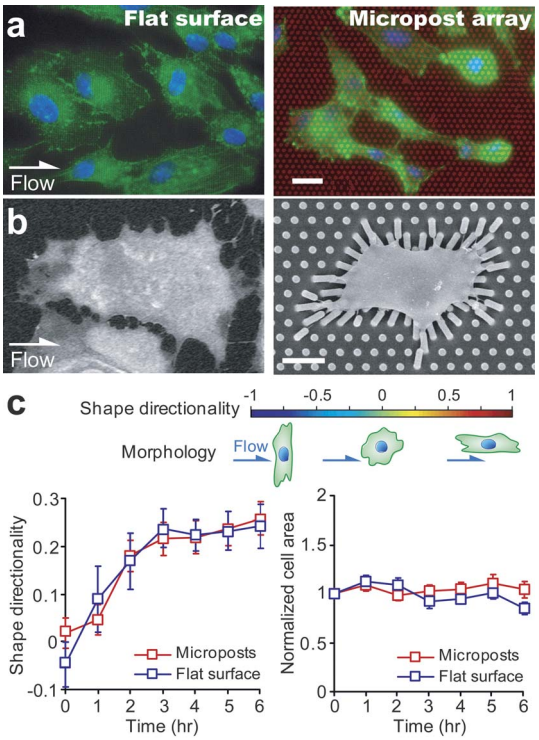

Fig. 4 Morphological response of single HUVECs under a constant shear stress of 20 dyne cm^{-2}. Immunostaining (a) and scanning electron microscopy (b) images of HUVECs after the 6 h shearing stimulation. The direction of the shear flow was from left to right, as indicated. *Left*: cells on the flat PDMS surface, *right*: cells on the PDMS micropost array. In (a), HUVECs were stained for the nucleus (*blue*) and actin microfilaments (*green*), and the PDMS microposts were stained with DiI (*red*). Scale bars, 20 μm (a) and 10 μm (b). (c) Temporal evolutions of the shape directionality (*left*) and normalized cell area (*right*) of individual HUVECs during the time course of the 6 h stimulation with the shear stress of 20 dyne cm^{-2}. The cell areas of single HUVECs were normalized to their baseline values measured right before the onset of the flow stimulation. Data represent the means ± SE (standard error) from 3 independent experiments, and cell number $n = 20$.

As shown in Fig. 5b, we observed that the shearing stimulation with $\tau_o = 20$ dyne cm^{-2} caused an instantaneous increase of CSK contractility of HUVECs and this heightened CSK contractility was sustained for about 4–5 h before it decreased gradually to its baseline value before the onset of shearing stimulation. The increase of CSK contractility of HUVECs during the first 4 h after the onset of shearing stimulation appeared to occur over the same period of time as the cells were dynamically regulating their morphology and became aligned and elongated in the direction of flow. Our observation here was not unexpected, as the critical involvement of CSK contractility in the shear-mediated morphological realignment process of ECs has been confirmed recently by others using pharmacological drugs to block myosin II activity and thus inhibit CSK contractility of ECs.[20,21,57] ECs with abolished CSK contractility do not activate the shear-mediated endothelial realignment process as compared to untreated controls.

The temporal evolution of the force directionality D in response to the sustained shearing stimulation is also plotted in

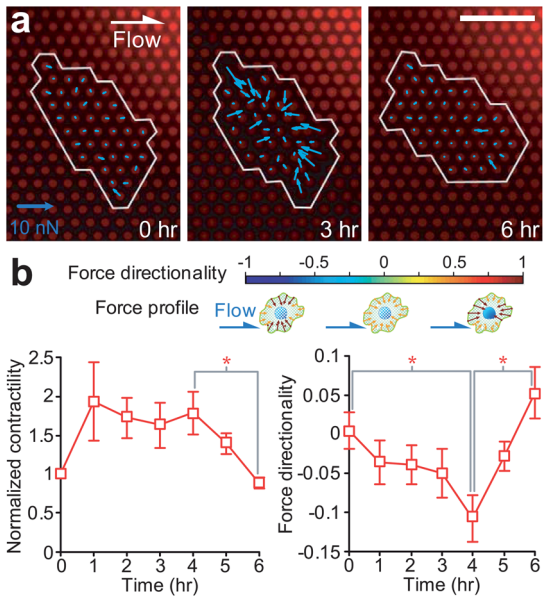

Fig. 5 Contractile response of single HUVECs under the constant shear stress of 20 dyne cm^{-2}. (a) Cellular traction force maps of a single HUVEC measured at different time points (*left*: 0 h, *middle*: 3 h, and *right*: 6 h) during the time course of the 6 h shearing stimulation. The cell periphery was outlined in white. The direction of the shear flow was from left to right, as indicated. Scale bar, 20 μm. (b) Temporal evolutions of the normalized cellular contractility (*left*) and force directionality (*right*) of individual HUVECs during the time course of the 6 h shearing stimulation. The cellular contractility of single HUVECs was normalized to the contractility baseline value measured right before the onset of the flow stimulation. Data represent the means ± SE from 3 independent experiments, and cell number $n = 20$. Statistical analysis was performed by employing Student's *t*-test. * indicates $p < 0.05$.

Fig. 5b. It appeared that during the first 4 h of the shearing stimulation with $\tau_o = 20$ dyne cm^{-2}, the force directionality D decreased monotonically from 0 to about −0.1. This decrease of the force directionality D occurred over the same period of time as the morphological realignment of HUVECs and their increase of CSK contractility. Interestingly, D rebounded and increased rapidly from −0.1 to 0.05 over the last 2 h of the shearing stimulation, during which period the CSK contractility of HUVECs decreased gradually to its baseline value to re-establish their tensional homeostasis.

Together, the dynamic responses of the CSK contractility and force directionality of HUVECs indicated that the cells could exert an orchestrated effort involving spatiotemporal regulation and reorganization of CSK structure and contractility to change their morphological features as response to directional shear stress. Our results showed that during the first 4 h of their morphological realignment process, HUVECs would extend their cell body along the direction of the flow while simultaneously contract in the direction perpendicular to the flow. The dynamic morphological change of HUVECs might be regulated or facilitated by the concurrent increase of their CSK contractility as well as a decrease of the force directionality D, both of which would contribute to enhanced and concentrated CSK contractile forces perpendicular to the flow direction, which might be necessary for breaking cell adhesions on the cell periphery perpendicular to the flow direction.

Conclusions

In this work, we reported an integrated microfluidic platform (the μPAC device) to study the shear-mediated endothelial mechanotransductive process. The PDMS micropost array incorporated in the μPAC device could serve as an effective structured surface to regulate both substrate rigidity and adhesive ECM pattern while simultaneously acting as force sensors to report live-cell subcellular CSK contractile forces. A novel soft lithography-compatible fabrication procedure was devised in this work for the μPAC device, in which a modified microcontact printing method was developed to coat the tops of the PDMS microposts inside the microfluidic channel with adhesive ECM molecules. Even though not directly relevant to investigations of the shear-mediated mechanotransductive process of ECs, using patterned microcontact printing, we further demonstrated that cell morphology and cell attachment locations could be controlled within the microfluidic channel of the μPAC device. Thus, the μPACs could potentially be integrated with other established microfluidic devices and components to provide a highly integrated microfluidic platform with a comprehensive control of both soluble and insoluble signals in the cellular microenvironment to facilitate investigations on mechanotransduction for different biological and biomedical applications.

To illustrate the general application of the μPAC device, we performed a detailed study of the shear-mediated endothelial mechanotransductive process. Our results showed that the cytoskeletal contractile forces of HUVECs were spatiotemporally regulated and coordinated to facilitate their morphological elongation process under a sustained shearing stimulation with $\tau_o = 20$ dyne cm^{-2}. The molecular mechanism that regulates involvements of CSK structure and contractility in the shear-mediated endothelial mechanotransductive process is not yet clear, and likely it will involve force-mediated FA dynamics and signaling.[20,21] Future investigations using the μPAC device with live-cell imaging of fluorescence-tagged FA proteins will help elucidate the molecular details of the FA-mediated mechanotransductive process in HUVECs and its spatiotemporal regulation and coordination with local CSK structure and contractility. Together, our work here might provide important insights into the shear-mediated mechanotransductive process of ECs, suggesting the importance of the spatiotemporal regulation and coordination of the CSK contractility in regulating the morphological response of ECs to the directional shearing stimulation.

Acknowledgements

We acknowledge financial support from the National Science Foundation (NSF CMMI 1129611), the National Institute of Health (UL1RR024986), and the department of Mechanical Engineering at the University of Michigan, Ann Arbor. We thank P. Mao for his assistance in microfabrication of the silicon micropost array master. We thank M. Yang and C. Chen for sharing the MATLAB program for quantifying cellular contractile forces. The Lurie Nanofabrication Facility at the University of Michigan, a member of the National Nanotechnology Infrastructure Network (NNIN) funded by the National Science Foundation, is acknowledged for support in microfabrication.

References

1 A. J. Engler, S. Sen, H. L. Sweeney and D. E. Discher, *Cell*, 2006, **126**, 677–689.
2 B. Geiger, J. P. Spatz and A. D. Bershadsky, *Nat. Rev. Mol. Cell Biol.*, 2009, **10**, 21–33.
3 V. Vogel and M. Sheetz, *Nat. Rev. Mol. Cell Biol.*, 2006, **7**, 265–275.
4 N. Wang, J. D. Tytell and D. E. Ingber, *Nat. Rev. Mol. Cell Biol.*, 2009, **10**, 75–82.
5 C. S. Chen, *J. Cell Sci.*, 2008, **121**, 3285–3292.
6 T. Mammoto and D. E. Ingber, *Development*, 2010, **137**, 1407–1420.
7 M. A. Wozniak and C. S. Chen, *Nat. Rev. Mol. Cell Biol.*, 2009, **10**, 34–43.
8 L. Wei, *et al.*, *Development*, 2002, **129**, 1705–1714.
9 R. Farhadifar, J. C. Roper, B. Aigouy, S. Eaton and F. Julicher, *Curr. Biol.*, 2007, **17**, 2095–2104.
10 Y. Numaguchi, *et al.*, *Angiogenesis*, 2003, **6**, 55–64.
11 A. Jacinto, *et al.*, *Curr. Biol.*, 2000, **10**, 1420–1426.
12 R. Bastock and D. Strutt, *Development*, 2007, **134**, 3055–3064.
13 A. Vasilyev, *et al.*, *PLoS Biol.*, 2009, **7**, e9.
14 A. J. Lusis, *Nature*, 2000, **407**, 233–241.
15 A. M. Malek, S. L. Alper and S. Izumo, *JAMA, J. Am. Med. Assoc.*, 1999, **282**, 2035–2042.
16 G. Dai, *et al.*, *Circ. Res.*, 2007, **101**, 723–733.
17 D. Pfander, B. Swoboda and T. Cramer, *Arthritis Res. Ther.*, 2006, **8**, 104.
18 F. A. Tylavsky, L. A. Spence and L. Harkness, *J. Nutr.*, 2008, **138**, 164S–165S.
19 S. E. Cross, Y. S. Jin, J. Rao and J. K. Gimzewski, *Nat. Nanotechnol.*, 2007, **2**, 780–783.
20 C. Hahn and M. A. Schwartz, *Nat. Rev. Mol. Cell Biol.*, 2009, **10**, 53–62.
21 K. A. Barbee, P. F. Davies and R. Lal, *Circ. Res.*, 1994, **74**, 163–171.
22 J. J. Paszkowiak and A. Dardik, *Vasc. Endovasc. Surg.*, 2003, **37**, 47–57.
23 S. Dimmeler, *et al.*, *Nature*, 1999, **399**, 601–605.
24 S. M. McCormick, *et al.*, *Proc. Natl. Acad. Sci. U. S. A.*, 2001, **98**, 8955–8960.
25 L. Hajra, *et al.*, *Proc. Natl. Acad. Sci. U. S. A.*, 2000, **97**, 9052–9057.
26 J. L. Lucitti, *et al.*, *Development*, 2007, **134**, 3317–3326.
27 F. Cosentino and T. F. Luscher, *J. Cardiovasc. Pharmacol.*, 1998, **32**(suppl. 3), S54–S61.
28 D. J. Hicklin and L. M. Ellis, *J. Clin. Oncol.*, 2005, **23**, 1011–1027.
29 F. Baffert, *et al.*, *Am. J. Physiol.: Heart Circ. Physiol.*, 2006, **290**, H547–H559.
30 A. Meeson, M. Palmer, M. Calfon and R. Lang, *Development*, 1996, **122**, 3929–3938.
31 J. W. Song, *et al.*, *Anal. Chem.*, 2005, **77**, 3993–3999.
32 T. D'Amico Oblak, P. Root and D. M. Spence, *Anal. Chem.*, 2006, **78**, 3193–3197.
33 E. W. Young, A. R. Wheeler and C. A. Simmons, *Lab Chip*, 2007, **7**, 1759–1766.
34 C.-J. Ku, T. D'Amico Oblak and D. M. Spence, *Anal. Chem.*, 2008, **80**, 7543–7548.
35 J. Shao, *et al.*, *Lab Chip*, 2009, **9**, 3118–3125.
36 J. W. Song, *et al.*, *PLoS One*, 2009, **4**, e5756.
37 S. Y. Hwang, *et al.*, *Anal. Chem.*, 2010, **82**, 3016–3022.
38 E. W. K. Young, M. W. L. Watson, S. Srigunapalan, A. R. Wheeler and C. A. Simmons, *Anal. Chem.*, 2010, **82**, 808–816.
39 J. L. Tan, *et al.*, *Proc. Natl. Acad. Sci. U. S. A.*, 2003, **100**, 1484–1489.
40 A. Saez, A. Buguin, P. Silberzan and B. Ladoux, *Biophys. J.*, 2005, **89**, L52–L54.
41 J. Fu, *et al.*, *Nat. Methods*, 2010, **7**, 733–736.
42 S. Weng and J. Fu, *Biomaterials*, 2011, **32**, 9584–9593.
43 M. T. Yang, J. Fu, Y. K. Wang, R. A. Desai and C. S. Chen, *Nat. Protoc.*, 2011, **6**, 187–213.
44 I. Wong and C.-M. Ho, *Microfluid. Nanofluid.*, 2009, **7**, 291–306.
45 Y. S. Li, J. H. Haga and S. Chien, *J. Biomech. Eng.*, 2005, **38**, 1949–1971.
46 Z. R. Healy, *et al.*, *Proc. Natl. Acad. Sci. U. S. A.*, 2005, **102**, 14010–14015.
47 M. L. Albuquerque, C. M. Waters, U. Savla, H. W. Schnaper and A. S. Flozak, *Am. J. Physiol.: Heart Circ. Physiol.*, 2000, **279**, H293–H302.
48 Y. C. Toh, K. Blagovic and J. Voldman, *Integr. Biol.*, 2010, **2**, 305–325.
49 R. H. Lam, M. C. Kim and T. Thorsen, *Anal. Chem.*, 2009, **81**, 5918–5924.
50 A. Brock, *et al.*, *Langmuir*, 2003, **19**, 1611–1617.
51 S. Miyamoto, *et al.*, *J. Cell Biol.*, 1995, **131**, 791–805.
52 D. Lehnert, *et al.*, *J. Cell Sci.*, 2004, **117**, 41–52.
53 M. Thery, *et al.*, *Nat. Cell Biol.*, 2005, **7**, 947–953.
54 B. J. Ballermann, A. Dardik, E. Eng and A. Liu, *Kidney Int., Suppl. (1974-2011)*, 1998, **67**, S100–S108.
55 E. Tzima, M. A. del Pozo, S. J. Shattil, S. Chien and M. A. Schwartz, *EMBO J.*, 2001, **20**, 4639–4647.
56 B. Wojciak-Stothard and A. J. Ridley, *J. Cell Biol.*, 2003, **161**, 429–439.
57 S. Chien, *Am. J. Physiol.: Heart Circ. Physiol.*, 2007, **292**, H1209–H1224.